

Performance Comparison of Frequency Domain Quadrupole and Dipole Electromagnetic Induction Sensors in a Landmine Detection Application

Eric B. Fails,^a Peter A. Torrione,^a Waymond R. Scott, Jr.^b and Leslie M. Collins^a

^aDepartment of Electrical Engineering, Duke University, Durham, NC 27708, USA;

^bSchool of Electrical and Computer Engineering at the Georgia Institute of Technology, Atlanta, GA 30332, USA

ABSTRACT

This work provides a performance comparison between two frequency-domain electromagnetic induction (EMI) sensors - one quadrupole and one dipole sensor for the detection of subsurface anti-personnel and anti-tank landmines. A summary of the physical differences between the two sensors and from those of other EMI sensors will be discussed. Previously we presented a performance analysis of the dipole sensor for a variety of detection algorithms over data collected at a government test facility indicating robust performance using the dipole sensor. The algorithms considered previously included an energy detector, matched subspace detector and a kNN probability density estimation approach over the features of a four parameter phenomenological model. The current sensor comparison will include, in addition to the previous detection methods, a Random Forests classification algorithm and utilize a larger training data set.

Keywords: Landmine, EMI, Detection, Pattern Recognition

1. INTRODUCTION

There are millions of buried landmines around the globe. These landmines maim or kill 15,000 - 20,000 victims per year. After many years of landmine remediation many countries have been declared mine-safe. As of 2004, Costa Rica, Djibouti, El Salvador, Kosovo and Moldova have all been declared mine safe.¹ An estimated 100,000 landmines are found and destroyed annually, while approximately 1.9 million new landmines are buried each year.² Landmines themselves are cheap to manufacture, nearly \$3, yet the cost of detection and remediation is about \$1000 per landmine.¹ Considering these cost estimates and the impact on local safety, agriculture and commercial/housing development one can see that buried landmines are a major problem.

Landmine remediation costs can be attributed to the extremely high false alarm rates associated with operating electromagnetic induction (EMI) sensors in energy detector mode. As a metal detector is tuned to be more sensitive to deeply buried mines or mines with little metallic content the sensor becomes more susceptible to errors from metallic clutter. These clutter items can include shrapnel, bullet casings as well as many other man made objects common to battlefields. Advancements in EMI landmine detection technology, data processing and classification algorithms attempt to improve performance, thus reducing clearance costs, by increasing the signal to noise ratio (SNR) and rejecting clutter items from misclassification.

The goals of this work are to produce a performance comparison between two specific frequency domain EMI sensors, developed at the Georgia Institute of Technology. This work will begin with an overview of the physical and output response differences between 2 wideband EMI (WBEMI) sensors, one dipole and one quadrupole. Next the characteristics of the test site, data collection and the signal model will be discussed in detail. Our initial comparisons will evaluate the EMI sensors' performances based upon baseline energy metrics and matched subspace detectors. Additional performance comparisons will be analyzed utilizing feature based classification methods. The WBEMI features will be discussed which will serve as the input to two classification techniques. The techniques chosen for this study are a class conditional density estimation technique utilizing information from the k-Nearest Neighbors of each class and Random Forests classification. The performance metrics for

Send correspondence to Leslie Collins, E-mail: lcollins@ee.duke.edu

comparison will be the receiver operating characteristic (ROC) curve, area under this ROC curve, and probability of false alarm (type 1 error) at the predetermined probability of detection of 95%. The objective of this study is to compare the performance of the EMI sensor types, not the detection/classification techniques. Because of the unknown nature of high dimensional feature spaces we will utilize multiple classification approaches to determine whether the dipole or quadrupole EMI sensor consistently outperforms the other. We will then conclude with a summary and analysis of these results.

2. WIDEBAND EMI SENSOR DESCRIPTIONS

In general, EMI sensors operate by emitting a time-varying electromagnetic (EM) field from a transmit coil and recording a secondary EM field in a receive coil. The primary EM fields produce eddy currents on the surface of buried conducting objects which produce time-varying EM fields of their own. These secondary fields are then recorded in the receive coil of the EMI sensor. The frequency domain EMI sensors considered here emit a multi-sine EM field over a broad range of the low frequency spectrum, which is chosen to correspond with the electrical lengths of targets of interest. By processing the received EM fields over these frequencies one can attempt to identify an object based on its frequency domain response. The fundamental concept in Electromagnetic Induction Spectroscopy (EMIS) is that an object's EMI frequency response is a function of geometry, material make-up, and orientation, which can uniquely identify a target.³



Figure 1. Wideband Electromagnetic Sensor Data Collection Systems (W. Scott, GA Tech)

The quadrupole and dipole EMI sensors being compared in this study are prototype systems being developed at the Georgia Institute of Technology and are shown in Fig. 1 mounted on a data collection cart.⁴ The prototype systems consist of sensor heads constructed using printed circuit board (PCB) technology. Each sensor head is shielded using PCB technology consisting of closely spaced conducting rings with a gap to avoid the completion of closed loops. This shielding reduces the amount of capacitive coupling between the sensor heads and nearby objects, while maintaining the inductive coupling to targets.⁵ The dipole sensor uses a simple dipole receive coil along with a secondary bucking transformer to cancel the inductive coupling between the transmit and receive coils.⁶ This configuration allows the system to have a simple detection region due to the dipole coils while benefiting from improved sensitivity due to cancellation from the ferrite core bucking transformer. The quadrupole sensor uses a quadrupole receive coil wound in a figure 8 pattern to cancel the mutual inductance between the transmit and receive coils, this sensor also utilizes the ferrite core output as a reference transformer. This configuration complicates the target response, and may reduce sensitivity to deeply buried targets relative to the dipole receive coil.⁵

3. EXPERIMENTAL SETUP, DATA CONSIDERATIONS AND PREPROCESSING

3.1. Test Facility

Data was collected at an Eastern United States government test facility. This test facility contains a variety of clutter items including metallic and non-metallic objects. Targets include anti-personnel metal and low metal (APM and APLM) landmines as well as anti-tank metal and low metal (ATM and ATLM) landmines. The clutter covers a wide range of objects, from large and small amounts of metal to various shapes and sizes of non-metallic clutter that are usually difficult for EMI sensors and ground penetrating radar (GPR) systems respectively. This facility consists of a number of lanes each divided into 1.5 x 1.5 m squares. Table 1 shows the distribution of the previously mentioned objects as well as blanks, locations where no object is buried. Notice that the distribution of targets at this test facility is weighted toward low metal and anti-personnel targets.

Table 1. Test Facility Distribution

Object Type	Proportion
APM	7%
APLM	23%
ATM	4%
ATLM	17%
Metallic Clutter	15.5%
Non-metallic Clutter	15.5%
Blanks	18%

The dipole sensor data includes two observations of this grid-based test facility in opposite directions. This data was collected in May 2007. Similarly, the quadrupole sensor data includes two observations also collected in opposite directions in October 2007.

3.2. Data

The data for both dipole and quadrupole sensors was collected at 21 frequencies that were approximately logarithmically spaced from 330 Hz to 90.03 kHz. The frequencies deviated from logarithmic spacing to minimize interference from power line harmonics. A multi-sine excitation signal was generated using the 21 frequencies and used to excite the EMI sensor. The response due to this multi-sine excitation was recorded in 0.1 s increments. These time records were transformed into the frequency domain and used to construct the frequency domain response of the sensor. Each 0.1 s windowed frequency domain data vector was then stamped with a down track (DT) spatial location within the grid square. The data collection carts and sensor heads traveled over each grid square at approximately 10 cm/s. Fig. 2 shows an example dipole EMI response of an ATM target buried at a depth of 5 in. The left image shows the imaginary EMI response over the entire grid square. The right image consists of the real and imaginary parts of the EMI response from the center DT location plotted separately.

3.3. Preprocessing

Linear background correction has been performed on the frequency domain data vectors as a preprocessing step at each DT location within a particular grid square. This simple background correction process consists of the subtraction of blank ground responses from the beginning of each grid location. Background correction helps mitigate sensor drift and changes in the ground response.

The final preprocessing stage consists of spatially filtering the response of each grid square in the down track direction. The filters attempt to further reduce the ground and sensor drift effects by attempting to increase the SNR by averaging data over several locations. The effects of the filters, as well as the complication and weakening of the quadrupole response relative to the dipole response are shown in Fig. 3.

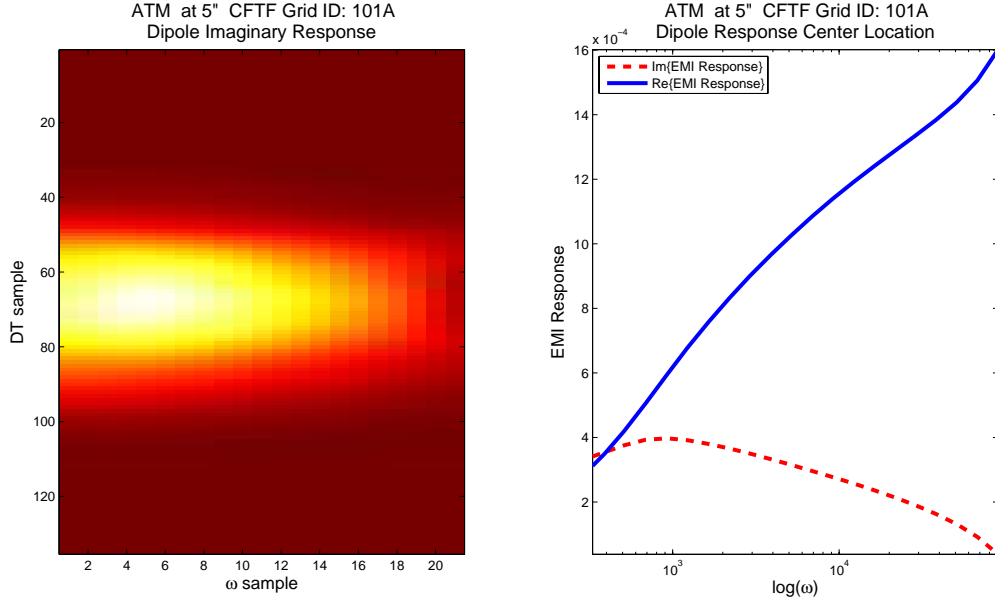


Figure 2. These images display an example WBEMI response from an metal anti-tank mine; the image on the left displays the imaginary response over an entire grid square, the image on the right displays the imaginary and real parts of the response at the center location of the grid square

4. SIGNAL MODEL

The signal model for the each grid square at the k^{th} DT location EMI response collected at the grid-based test facility is,

$$\mathbf{x}_k = \mathbf{r}_k + \mathbf{g}_k + \mathbf{n}_k$$

where \mathbf{x} is the received signal, \mathbf{r} is the target signal, \mathbf{g} is the ground response and \mathbf{n} is additive noise. Our objective for detection is to determine whether or not \mathbf{r} is present. Each vector is sampled at the 21 frequencies mentioned in Sect. 3.2, $x_{ik} = x_k(\omega_i) : i \in [1, 21]$. Rather than processing the data vector from the physical center of the grid square one can process the data vector which has the most energy. We have chosen to process the data vector at the DT location, K , which is chosen as the maximum imaginary energy down track location in the particular grid square.

$$K = \operatorname{argmax}_k \left(\sum_{i=1}^{21} \Im\{x_{ik}\}^2 \right)$$

The ground response \mathbf{g} and noise \mathbf{n} are partially removed by background (ground response of a known blank location in proximity to the grid square of interest) subtraction and filtering discussed in Sect. 3.3. From this point forward the signals, \mathbf{x} , we are working with represent the background subtracted, filtered response of a grid square at the maximum imaginary energy down track location K .

5. BASELINE COMPARISONS

In order to get an effective initial glance of the dipole and quadrupole EMI sensors' performances, we will compare their energy detector performances. This is a common EMI operation mode (metal detector) for landmine detection. Although not typically considered a baseline detector, the matched subspace detector performance of the sensors will also be compared. This is due to the robustness of this approach for landmine detection.⁷ Also, both of these methods utilize the entire data vector, $\mathbf{x} \in \mathbb{C}^{21}$ for each grid square, while the feature based classification methods of Sect. 6 operate on a feature space for $\mathbf{z} \in \mathbb{R}^5$, where $\mathbf{z} = f(\mathbf{x})$.

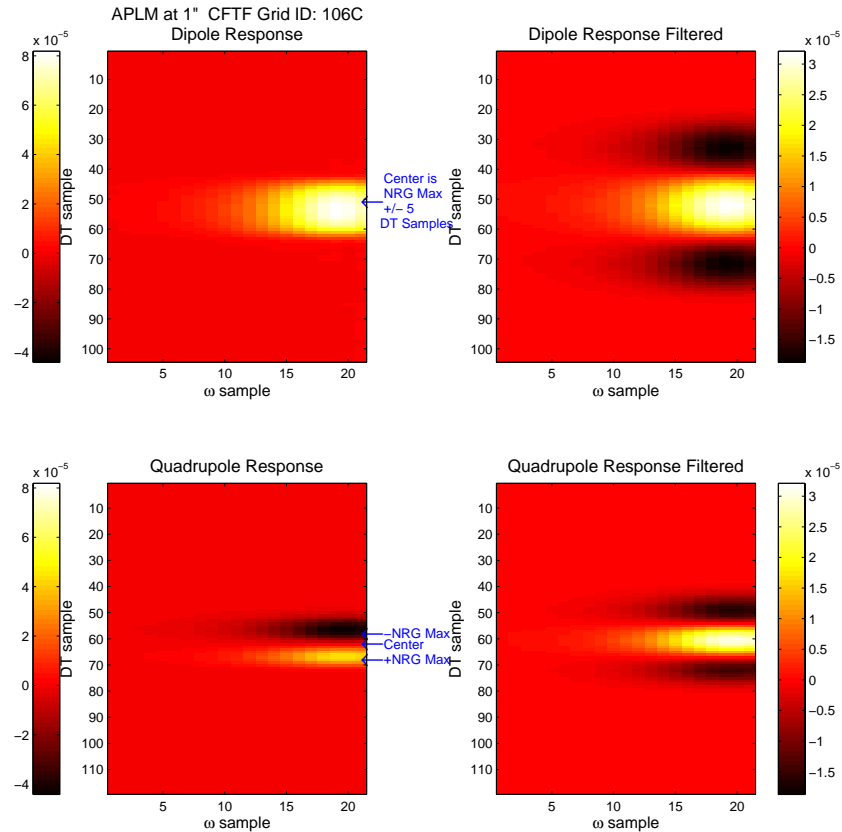


Figure 3. These images display the complication and weakening of the quadrupole detection zone relative to the dipole discussed in Sect. 2 and the effect of spatially filtering

5.1. Energy Detector

Because of the complex nature of EMI responses, we have chosen to process the in-phase (real) and quadrature (imaginary) energies separately. The real energy detector is defined as,

$$E_{ip} = \sum_{i=1}^{21} \Re\{x_i\}^2$$

where the energy is the sum of the squares of the real part of the data vector \mathbf{x} over the 21 frequencies indexed by i . The imaginary energy detector is defined as,

$$E_q = \sum_{i=1}^{21} \Im\{x_i\}^2$$

where the energy is the sum of the squares of the imaginary part of the data vector \mathbf{x} over the 21 frequencies indexed by i . The energy detector ROC curve results and 95% confidence intervals for the two sensors are shown in Fig. 4. Additional performance metrics are included in the ROC curve legends and in Table 2 of Sect. 7.

5.2. Matched Subspace Detector

The dipole and quadrupole sensor performances will be compared by the well-known matched subspace detector,^{8,9} which has previously shown good performance on WBEI data.^{10,11} The matched subspace detection algorithm for WBEI responses begins by estimating the subspace for each landmine type. Because the quadrature responses of particular landmine types are scaled, based on depth, versions of one another the mine type

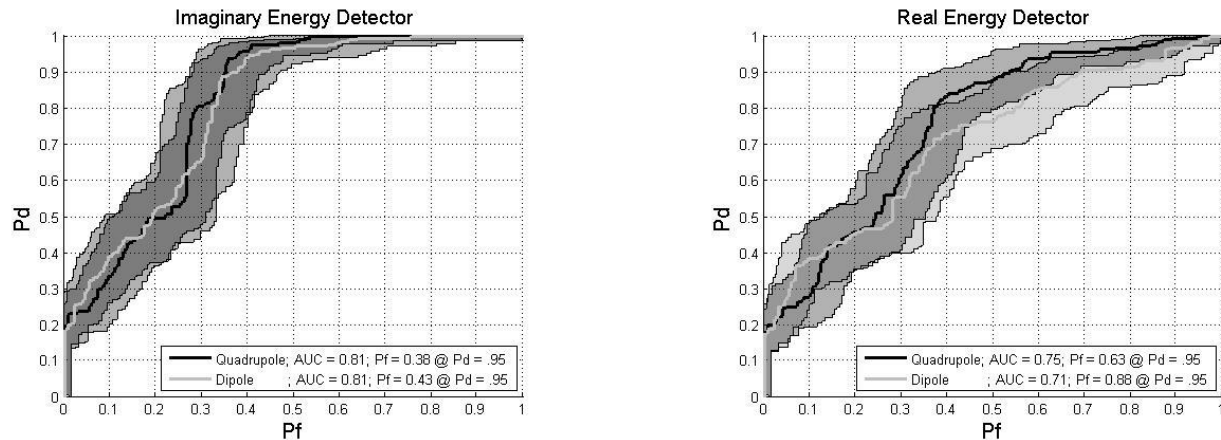


Figure 4. Energy Detector Empirical ROC Results; The areas under the imaginary energy detector ROC curve (AUC) for both sensors are comparable, while the AUC for the real energy detector indicates better quadrupole sensor performance.

signal subspace is estimated as the average of the normalized quadrature responses for the particular mine type in the training data.^{10,11} Next, the algorithm requires the creation of projection matrices for each mine type subspace estimate. The projection matrices onto these subspaces are defined as

$$\mathbf{P}_H = \mathbf{H}(\mathbf{H}^T \mathbf{H})^{-1} \mathbf{H}^T$$

where \mathbf{H} is the subspace estimate for a particular mine type and the superscript T represents transpose. During the training phase the minimum and maximum quadrature energies from each mine type in the training data are maintained for the detect process. Because the training data set consists of two observations of the same test facility, cross validation is performed as leave “two” out, i.e. both observations of the grid square being tested are left out of the training data.

The matched subspace detect process for WBEMI responses is two tier. The first tier consists of a pre-screening energy detector. If the quadrature energy of the test vector falls below a certain multiple of the minimum quadrature energy or above a multiple of the maximum quadrature energy for a particular mine type in the training set, the decision statistic for that mine type is assigned a value of 0. The scale factor used in this work is 2. This energy detection helps to prevent the misclassification of clutter that appears as scaled versions of the landmine type subspace. Otherwise, the quadrature part of the test vector is passed on to the second tier of our detector where the cosine decision statistic^{8,9} is computed for the landmine type subspace.

$$\lambda = \frac{\mathbf{x}^T \mathbf{P}_H \mathbf{x}}{\mathbf{x}^T \mathbf{x}}$$

This process is performed in parallel for each land mine type subspace, a matched subspace detector bank. The matched subspace detector performance could possibly be enhanced through the creation of a blank, metallic and nonmetallic clutter projection matrices. The matched subspace detector ROC curve results and 95% confidence intervals for the dipole and quadrupole sensors are shown in Fig. 5. Additional performance metrics are included in the ROC curve legend and in Table 2 of Sect. 7.

6. FEATURE BASED CLASSIFICATION PERFORMANCE COMPARISONS

To further analyze the effectiveness of the dipole and quadrupole sensors we will evaluate them on feature based classification performance. These methods have been shown to be capable of improving EMI landmine detection performance, by discriminating between landmine targets and metallic clutter objects.^{3,7,12-16}

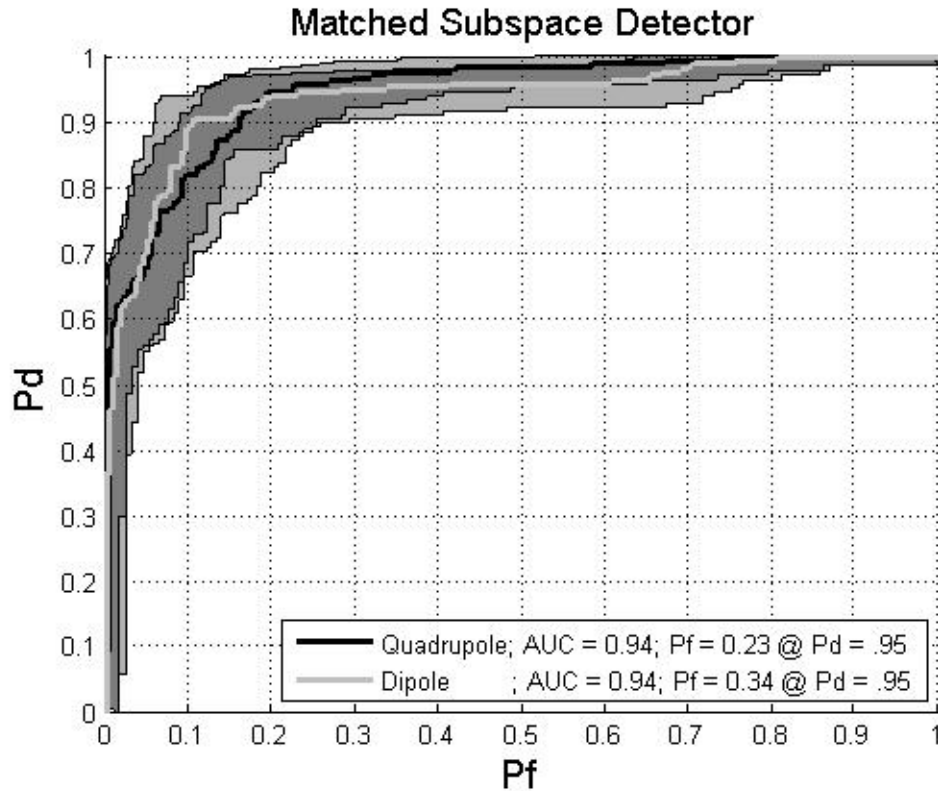


Figure 5. Matched Subspace Detector Empirical ROC Results; The area under the matched subspace detector ROC curve (AUC) for both sensors are comparable.

6.1. Features

The features used in this study, developed by Miller et. al.,¹⁷ have been used in our previous work.¹⁸ The four parameter phenomenological model resulting in these features has been shown by Miller et. al. to be very accurate for objects of high permeability in the high frequency range of the response. The underlying signal response of an object for the model being considered is

$$S(\omega) = A(X(\omega) + jY(\omega))$$

in which A , the amplitude is dependent on object geometry and field strength, while $X(\omega) + jY(\omega)$ is the frequency dependent component. This response is highly dependent upon the geometry and material structure of the object. The underlying model is based upon the relation between the known response of spheres and cylinders discussed by Grant and West.¹⁹ It is interesting to note that the four parameter model is an extension of this relation, giving consideration to objects of non-compact shape. The parametric model under consideration is

$$X(\omega) + jY(\omega) = q \left(s + \frac{(j\omega\tau)^c - 2}{(j\omega\tau)^c + 1} \right)$$

where the parameter q represents amplitude, τ is a time constant, s controls the asymptotes at low and high frequencies while the parameter c controls the width of the transition zone.¹⁷ This parametric model is fit to the observation vectors, \mathbf{x} , using an iterative nonlinear least squares regression technique. The four parameters are then \log_{10} scaled. The quadrature energy discussed in Sect. 5.1 is used as an additional feature resulting in a length $d = 5$ feature vector, $\hat{\mathbf{z}} = [\hat{q}, \hat{t}, \hat{s}, \hat{c}, E_q] \in \mathbb{R}^5$, where the carat notation indicates estimated values.

6.2. kNN Density Estimate

Density estimation techniques that utilize the k Nearest Neighbors (kNN) at a continuity point have been studied extensively.²⁰ The non-parametric density estimation technique discussed here is based upon the original work of Fix and Hodges, and weighted nearest neighbor rules. These works suggest that the volume of a region enclosing the kNN of a point, \mathbf{x} , can be used to estimate the point's probability density,²¹

$$p(\mathbf{x} | H_i) \approx \frac{k/n_i}{V_i} \text{ for } i = 0, 1$$

where n_i and V_i are the total number of training points and volume of the region enclosing k neighbors from class i respectively. We have limited our notation to a two-class problem. The weighted nearest neighbor rules suggest that weighting the neighbors based upon distance to the test point can lead to better performance with finite training data sets.

The approach used here begins by calculating the average distance to the kNN from each class,

$$r_i = \frac{1}{k} \sum_{j=1}^k d_{ij} \text{ for } i = 0, 1$$

where d_{ij} is the distance to the j^{th} nearest neighbor for class i . The Euclidean distance metric is used in this work. Using the average distance is similar to the kNN rule introduced by Hattori and Takahashi²⁰ with $\ell = 1$, weighting each of the j neighbors solely on their distance. This average distance is then used to estimate the expected volume which encloses the k neighbors. The class conditional density estimate for our feature vector, \mathbf{z} is,

$$\hat{p}(\mathbf{z} | H_i) = \frac{k/n_i}{c r_i^d} \text{ for } i = 0, 1$$

where $c = \frac{\pi^{\frac{d}{2}}}{\Gamma(\frac{d}{2}+1)}$ is the volume scaling factor for a d-dimensional hypersphere.

Since we are dealing with a two class detection problem we will estimate the likelihood ratio using the class conditional density estimates from the kNN of each class is,

$$\begin{aligned} \hat{\lambda} &= \frac{\hat{p}(H_1 | \mathbf{z})}{\hat{p}(H_0 | \mathbf{z})} \\ &= \frac{\frac{\hat{p}(\mathbf{z}|H_1)\hat{p}(H_1)}{p(\mathbf{z})}}{\frac{\hat{p}(\mathbf{z}|H_0)\hat{p}(H_0)}{p(\mathbf{z})}} \\ &= \frac{\frac{k/n_1}{p(\mathbf{z})c r_1^d} \frac{n_1}{N}}{\frac{k/n_0}{p(\mathbf{z})c r_0^d} \frac{n_0}{N}} \\ &= \left(\frac{r_0}{r_1} \right)^d \\ &= \left(\frac{\sum_{j=1}^k d_{0j}}{\sum_{j=1}^k d_{1j}} \right)^d \end{aligned}$$

where $N = n_0 + n_1$, is the total number of training points. This corresponds to the weighted kNN rule proposed by Hattori and Takahasi²⁰ with $\ell = 1$. The log likelihood ratio estimate is $\hat{\lambda} = \log(r_0) - \log(r_1) = \log \left(\sum_{j=1}^k d_{0j} \right)$

- $\log \left(\sum_{j=1}^k d_{1j} \right)$. The kNN density estimation ROC curves results and 95% confidence intervals for the dipole and quadrupole sensors are shown in Fig. 6 for $k = 7$ and $k = 9$. Additional performance metrics are included in the ROC curve legend and in Table 2 of Sect. 7. Judging from AUC and confidence regions, the performance of both sensors are comparable.

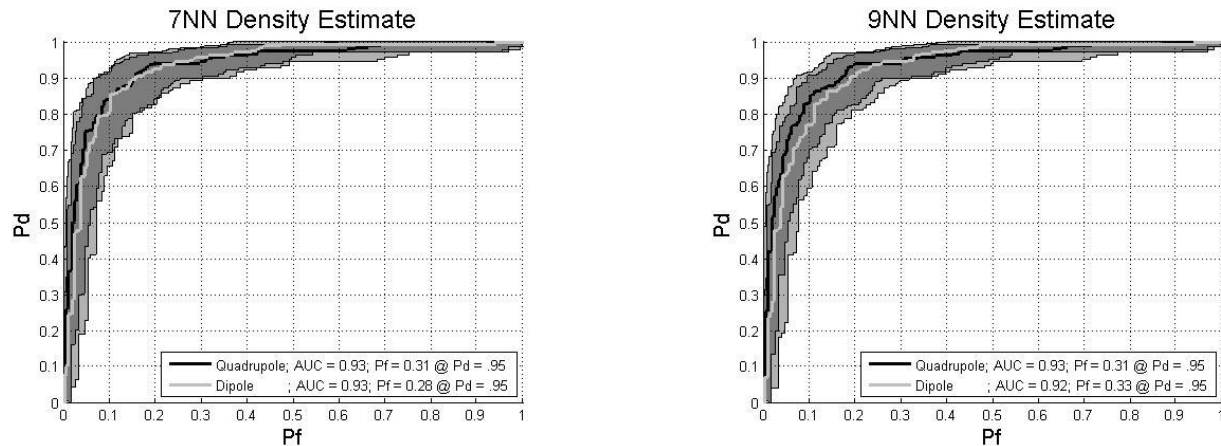


Figure 6. kNN Density Estimate Empirical ROC Results; The area under the 7NN and 9NN detector ROC curve (AUC) for both sensors are comparable.

6.3. Random Forests

Random Forest²² classification and regression is an ensemble method which combines CART (Classification and Regression Trees),²³ random subspace projection,²⁴ bagging, and bootstrapping. This method is very accurate compared to current algorithms over classical data sets and handles high dimensional data inherently well. The Random Forests algorithm involves growing n CARTs (n trees in the forest) without pruning. The training data for each tree consists of bootstrap samples drawn with replacement from the full training data set. At each node in a decision tree, split on $m \ll d$ randomly selected features. The weightings on the m features are determined by the best split over the residual training data at the node. The test data are then input to each tree in the forest, one can then use the proportion of the n tree “votes” for each class as the posterior density estimate for the particular test point. For this study, values of $n = 1000$, number of trees in forest, and $m = 3$, node split vector length, were used. We then threshold these posterior density estimate values to generate the ROC curve and 95% confidence intervals for the dipole and quadrupole sensors in Fig. 7. Additional performance metrics are included in the ROC curve legend and in Table 2 of Sect. 7. Judging from AUC and confidence regions, the performance of both sensors are comparable.

7. SUMMARY AND CONCLUSIONS

The results from each of the performance comparisons are summarized in Table 2. It appears from analyzing the data and energy detector results that the quadrupole sensor may have higher SNR. However, further classification results indicate highly comparable performance among the dipole and quadrupole EMI sensors when evaluating performance based upon AUC and giving consideration to ROC 95% confidence regions. We conclude that the performance results of both the dipole and quadrupole WBEMI sensor designs implemented by the Georgia Institute of Technology indicate robust performance for landmine detection.

ACKNOWLEDGMENTS

This work was supported under a grant from the US Army RDECOM CERDEC Night Vision and Electronic Sensors Directorate (NVESD). The authors would also like to thank our colleagues at the Georgia Institute of

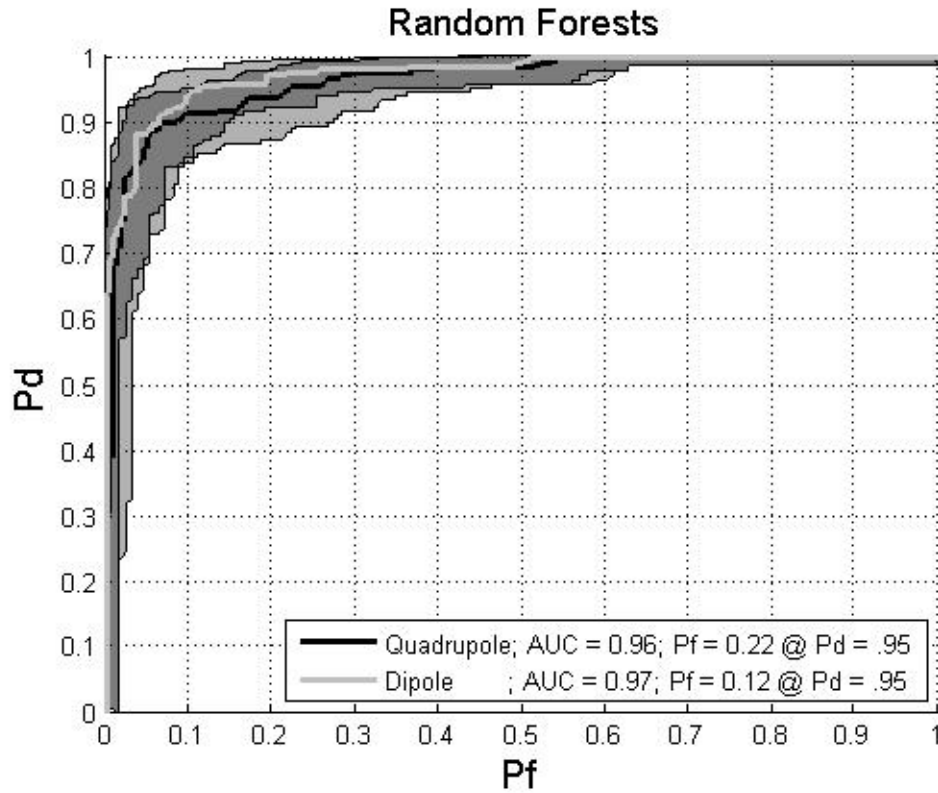


Figure 7. Random Forests Classification Results; The area under the Random Forests Classifier ROC curve (AUC) for both sensors are comparable.

Table 2. Results Summary

Detector	Dipole AUC	Quad AUC	Dipole Pf @ Pd = .95	Quad Pf @ Pd = .95
Real Energy	.71	.75	.88	.63
Imaginary Energy	.81	.81	.43	.33
Matched Subspace Detector	.94	.94	.34	.23
7NN	.93	.93	.28	.31
9NN	.92	.93	.33	.31
Random Forests	.97	.96	.12	.22

Technology, University of Florida, Niitek, Institute for Defense Analysis (IDA) and NVESD for their contributions to this work.

REFERENCES

1. "Adopt a minefield," <http://www.landmines.org/> , 2007.
2. J. MacDonald, *Alternatives for Landmine Detection*, RAND, 2003.
3. D. Keiswetter, I. Won, J. Miller, T. Bell, E. Cespedes, and K. O'Neill, "Discriminating capabilities of multifrequency emi data," in *Geoscience and Remote Sensing Symposium, 2000. Proceedings. IGARSS 2000. IEEE 2000 International*, 4, pp. 1415–1417vol.4, 24-28 July 2000.

4. J. Waymond R. Scott, "Personal communication." Field Data for the Wideband EMI Detector, December 2007.
5. W. R. Scott, "Broadband electromagnetic induction sensor for detecting buried landmines," *Geoscience and Remote Sensing Symposium, 2007. IGARSS 2007. IEEE International*, pp. 22–25, 23–28 July 2007.
6. W. R. Scott, Jr. and M. Malluck, "New cancellation technique for electromagnetic induction sensors,," in *Proceedings of the SPIE: 2005 Annual International Symposium on Aerospace/Defense Sensing, Simulation, and Controls*, **5794**, April 2005.
7. P. Torrione and L. Collins, "Performance comparison of automated induction-based algorithms for landmine detection in a blind field test," *Subsurface Sensing Technologies and Applications* **5**, pp. 121–150, July 2004.
8. L. Scharf and B. Friedlander, "Matched subspace detectors," *Signal Processing, IEEE Transactions on [see also Acoustics, Speech, and Signal Processing, IEEE Transactions on]* **42**, pp. 2146–2157, Aug. 1994.
9. L. Scharf, *Statistical Signal Processing: Detection, Estimation, and Time Series Analysis*, Reading MA: Addison Wesley, 1991.
10. P. A. Torrione, "A comparison of statistical algorithms for landmine detection," Master's thesis, Duke University, 2002.
11. P. A. Torrione and L. M. Collins, "Performance of matched subspace detectors and support vector machines for induction-based land mine detection," in *Proceedings of SPIE*, J. T. Broach, R. S. Harmon, and G. J. Dobeck, eds., *Detection and Remediation Technologies for Mines and Minelike Targets VII* **4742**, pp. 800–811, SPIE, August 2002.
12. T. Bell, B. Barrow, and J. Miller, "Subsurface discrimination using electromagnetic induction sensors," *IEEE Transactions on Geoscience and Remote Sensing* **39**, pp. 1286–1293, June 2001.
13. L. Collins, P. Gao, and S. Tantum, "Model-based statistical signal processing using electromagnetic induction data for landmine detection and classification," in *Proceedings of the 11th IEEE Signal Processing Workshop on Statistical Signal Processing*, pp. 162–165, 6–8 Aug 2001.
14. L. Collins, P. Gao, D. Schofield, J. Moulton, L. Makowsky, D. Reidy, and R. Weaver, "A statistical approach to landmine detection using broadband electromagnetic induction data," *IEEE Transactions on Geoscience and Remote Sensing* **40**, pp. 950–962, April 2002.
15. P. Gao, L. Collins, N. Geng, L. Carin, D. Keiswetter, and I. Won, "Classification of landmine-like metal targets using wideband electromagnetic induction," in *ICASSP '99 Proceedings., 1999 IEEE International Conference on Acoustics, Speech, and Signal Processing*, **4**, pp. 2327–2330 vol.4, 15–19 March 1999.
16. N. Geng, P. Garger, L. Collins, L. Carin, D. Hansen, D. Keiswetter, and I. Won, "Wideband electromagnetic induction for metal-target identification: Theory, measurement, and signal processing," in *Proceedings of SPIE, Detection and Remediation Technologies for Mines and Minelike Targets III* **3392**, SPIE, Sept 1998.
17. J. Miller, T. Bell, J. Soukup, and D. Keiswetter, "Simple phenomenological models for wideband frequency-domain electromagnetic induction," *IEEE Transactions on Geoscience and Remote Sensing* **39**, pp. 1294–1298, June 2001.
18. E. Fails, P. Torrione, W. R. Scott Jr., and L. Collins, "Performance of a four parameter model for modeling landmine signatures in frequency domain wideband electromagnetic induction detection systems," in *Proceedings of SPIE*, R. S. Harmon, J. T. Broach, J. H. Holloway, and Jr., eds., *Proceedings of SPIE, Detection and Remediation Technologies for Mines and Minelike Targets XII* **6553**, p. 65530D, 2006.
19. F. Grant and G. West, *Interpretation Theory in Applied Geophysics*, New York: McGraw-Hill, 1965.
20. K. Hattori and M. Takahashi, "A new nearest-neighbor rule in the pattern classification problem," *Pattern Recognition* **32**, pp. 425–432, March 1999.
21. R. O. Duda, P. E. Hart, and D. G. Stork, *Pattern Classification*, New York: Wiley, 2 ed., 2001.
22. L. Breiman, "Random forests," *Machine Learning* **45**, pp. 5–32, 2001.
23. L. Breiman, J. H. Friedman, R. A. Olshen, and C. J. Stone, *Classification and regression trees*, Brooks/Cole Publishing, 1984.
24. T. K. Ho, "The random subspace method for constructing decision forests," *IEEE Trans. on Pattern Analysis and Machine Intelligence* **20 (8)**, pp. 832–844, 1998.